Dual-Gate Organic Electrochemical Transistors Based on Laser-Scribed Graphene for Detecting Dopamine and Glutamate

*Yao Yao, Farzam Alimardani, Ping Ren, Jingyan Dong, SungHo Lee, Yuan-Shin Lee, Yi Wang**

Yao Yao
University of Missouri, Columbia, MO, 65201, United States
Farzam Alimardanikhaslouei
University of Missouri, Columbia, MO, 65201, United States
Ping Ren
Kettering University, United States, Flint, Michigan, 48504, United States
Jingyan Dong
North Carolina State University, Raleigh, NC, 27606, United States
Yuan-Shin Lee
North Carolina State University, Raleigh, NC, 27606, United States
SungHo Lee
University of North Carolina, Chapel Hill, NC, 27599, United States

Yi Wang
University of Missouri-Columbia, MO, 65211, United States
E-mail: yiwang@missouri.edu

Abstract

Organic electrochemical transistors (OECTs) are gaining significant attention due to their high sensitivity, customizability, ease of integration, and low-cost manufacturing. In this paper, we designed and developed a flexible dual-gate OECT based on laser-scribed graphene (LSG) with modified OECT gates for the simultaneous detection of dopamine and glutamate, two critical neurotransmitters. The developed OECTs are fully carbon-based and environmentally friendly. By modifying one gate with biopolymer chitosan for dopamine detection and the other with L-Glutamate oxidase enzyme for glutamate detection, we successfully achieved highly selective and sensitive measurements with detection limits of 5 nM for dopamine and 0.1 μM for glutamate. The modified dual-gate shows no interference between the detections of two neurotransmitters, making it a promising tool for customized multi-neurotransmitter analysis.

The results demonstrate the potential of LSG-based OECTs in customizable biosensing applications, offering a flexible, cost-effective platform for biomedical disorder diagnostics.

Keywords: OECT, LSG, PEDOT:PSS, Neurotransmitters, Dopamine, Glutamate, Neural Chemical Sensors

1. Introduction

Neurotransmitters (NTs) are released upon the arrival of action potentials, such as dopamine and glutamate, which play a crucial role in transmitting signals between neurons and other cells for regulating biological processes and behaviors [1]. For instance, glutamate is one of the most prominent excitatory NTs, which plays a crucial role in regulating emotional, cognitive, and motor functions [2]. In addition, dysfunction of dopaminergic neurotransmission caused by abnormal metabolism or neuronal imbalance would lead to many neurological disorders [3,4], such as Parkinson's disease, autism, and schizophrenia. Notably, the clinical concentrations of these NTs in the animal's body are typically very low. Accurately measuring these NTs in real-time is essential for understanding the mechanisms of our nervous system and for treating challenging neurological diseases, such as Parkinson's disease, Alzheimer's disease, depression, etc. [4–6]

To precisely measure the NTs *in vivo* or *in vitro*, researchers have reported a variety of techniques, including high performance liquid chromatography (HPLC), mass spectrometry imaging (MSI), and electrochemical analysis, etc. Using HPLC to measure dopamine or glutamate involves microdialysis process, which requires the collection and preparation of brain samples in the beginning [7]. While HPLC allows a very low detection limit, it can only resolve averaged biochemical events over minutes and has relatively poor spatial resolution. Moreover, the measurement procedure is technically complex and time-consuming, and it usually needs to be performed in a laboratory setting with expensive instruments. MSI allows spatially correlated mass spectrometry analysis to simultaneously assess the distributions of panels of NTs, such as dopamine, amino acid, and acetylcholine [8]. However, accurate quantification of NTs using MSI could be difficult and unsuitable for portable and low-cost analytical measurement. Electrochemical analytical techniques, such as amperometry and cyclic voltammetry (CV), for NT measurement, are attractive due to their low cost, ease of operation, high sensitivity, fast response, and potential for miniaturization [9,10]. Cyclic voltammetry (CV) was extensively employed to monitor NTs, such as dopamine and glutamate, by recording

oxidation-induced changes in related current-voltage curves [11,12]. While this technique is efficient and can be NT selective, the readout from the CV is not intuitive. In addition, the technique also involves a complex instrument configuration [13], which increases the challenge of minimization for wearable devices. Recently, transistors as amplifying transducers, coupled with electrochemical mechanisms, have been developed to measure NTs released in a living animal's brain. For instance, field effect transistors (FETs) have been developed for *in vivo* detection of dopamine and other neurotransmitters as small molecule analytes [14]. During the operation of FETs, as doping changes occur only in a thin interfacial region adjacent to the gate dielectric, their amplifying performance is limited. Contrary to FETs, Organic electrochemical transistors (OECTs) have emerged as promising transducers for detecting chemical, electrical, and molecular signals [12,15–18], in which doping occurs throughout the entire volume of the channel. Compared to other types of organic field-effect transistors (OFETs), OECTs can operate at low voltages (below 1V [6,19]) with outstanding amplification capability and efficient ion transport/exchange between the device and electrolyte environment [20]. OECTs are increasingly gaining attention in electrochemical sensing [21,22] and biosensing applications [23–25] due to their excellent biocompatibility and simple fabrication.

The basic configuration of an OECT consists of source, drain, and gate electrodes, with an organic semiconductor channel bridging the source and drain. This channel can be made of either a p-type organic material that conducts holes or an n-type organic material that conducts electrons. A distinguishing feature of OECTs, compared to OTFTs, is the use of an electrolyte between the channel and the gate instead of a dielectric material directly contacting the gate. This electrolyte facilitates electrochemical, catalytic, or enzyme-catalyzed reactions on the gate electrode surface. When a voltage is applied between the source and drain, a drain current flows through the conductive channel, which is subsequently transformed into an amplified signal of the drain current. Furthermore, electrolyte-mediated gating allows for the development of simple, planar device architectures with the gate electrode patterned next to the channel, thereby simplifying the fabrication process. Importantly, the gate surface can be modified to detect different small biomolecules, providing adaptability and customizability in biosensing applications for simultaneous multimodal signal detections.

Conventional processes for the fabrication of OECTs are based on surface micromachining techniques, such as physical/chemical vapor deposition, photolithography, and etching processes. The strong acidic and alkaline solutions used for micromachining would damage the fabricated organic polymer channels and biorecognition element modified gate (such as enzymes), causing the failure of OECTs. Moreover, conventional OECTs use silver (Ag),

platinum (Pt), or gold (Au) as the source, drain, and gate materials due to their excellent electrical conductivity. However, they are also expensive and rely on complicated deposition facilities [26]. The rigid mechanical properties of these metals also make them not good for flexible electronics. Additionally, specific masks must be designed and fabricated to pattern the electrodes. Besides the complexity of the manufacturing process and material waste, it also significantly limits the customizability of biosensors, making it difficult to meet the development of OECTs in biosensor applications. In order to address these issues, this paper explored the potential of Laser-Scribed Graphene (LSG) to replace the traditional noble metals as source, drain, and gate electrodes of OECTs to fabricate highly customizable neurochemical sensors. LSG is produced through direct laser writing on commercially available polyimide sheets, exhibiting outstanding physicochemical characteristics, including high electronic conductivity, excellent thermal conductivity, exceptional mechanical strength, and biocompatibility [27]. The high porosity and high conductivity of LSG also enable OECTs to have excellent sensing properties.

In this paper, we present a simple and cost-effective approach to designing and fabricating flexible OECTs with dual-gates structures for rapid NT sensing. The LSG processing parameters were investigated and optimized for the electrode fabrication of the OECTs. We also studied the modification methods for the gate electrodes using biopolymer and enzyme, enabling simultaneous measurement of different NTs. The in vitro experiments demonstrate that gate modified OECTs possess excellent selectivity and sensitivity, which is promising for various biosensing applications with a low-cost, customizable, and environmentally friendly manufacturing framework.

2. Results and Discussion

2.1. LSG-based Dual-gate OECT

By leveraging the working principle of the OECT, a dual-gate OECT structure is designed, as shown in **Figure 1a**, in which the OECT can be customized to measure two different NTs by modifying the gates and sharing the same source and drain electrodes. This design allows for maximized functionality of the OECT while minimizing its footprint. In order to achieve a highly customizable and cost-effective method to produce dual-gate OECTs for various applications, all the electrodes of the OECT are fabricated using LSG on commercially available polyimide (PI) thin film with a benchtop UV laser cutter.

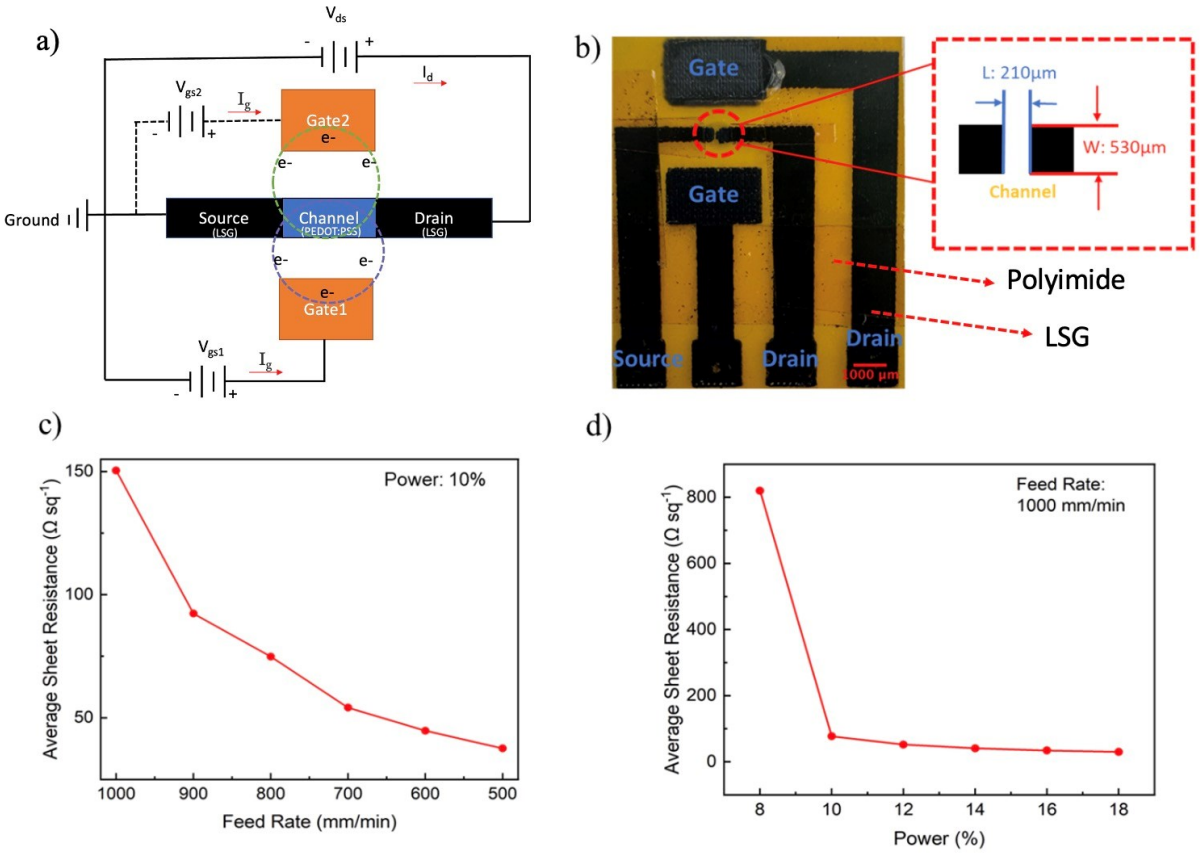

Figure 1. a) Schematic diagram of an LSG-based OECT design with dual gates structure. b) Photo of LSG-based OECT with the channel design. c) Relationship between sheet resistance of LSG and laser scribing feed rate. d) Relationship between sheet resistance of LSG and laser power.

The channel geometry directly influences the performance of the OECT, such as transconductance (g_m). In this paper, the design of the channel geometry was guided by Rivnay's model, as shown in Equation (1).

$$g_m = \frac{W}{L} \cdot d \cdot \mu \cdot C^* \cdot (V_{th} - V_g) \quad (1)$$

Where channel dimensions W = width, L = length, d = thickness of channel, μ is hole mobility, C* is volumetric capacitance, and V_{th} and V_g are the threshold and gate voltage, respectively. According to the equation, to increase the transconductance g_m, the W/L ratio needs to be sufficiently large within a certain range. However, the length between the source and drain electrodes is limited by the resolution of benchtop laser cutting. After multiple trials, we determined the optimal aspect ratio parameters for the fabricated OECT channel: 210 μm in length and 530 μm in width, as shown in **Figure 1b**.

The LSG is fabricated on 0.0010" thick polyimide film using a benchtop 5W UV laser cutter. According to previous research [28], the electrical conductivity of LSG is related to the laser

power absorbed by the polyimide film. Higher laser power and lower scribing speed result in a thicker LSG layer, leading to improved electrical conductivity. However, the thin polyimide film is chosen, which will be easy to burn through with high laser power and slow engraving speed, causing fabrication failure. In this paper, characterization experiments of LSG were conducted with different engraving parameters. Laser power was selected in the range of 8% to 18%, with a laser feed rate of 500 to 1000 mm/min. The corresponding sheet resistances were then measured using a Keithley 2410 instrument with a four-point probe method, as shown in **Figures 1(c) and (d)**. When setting a constant power (10% power in **Figure 1(c)**), decreasing the feed rate causes a thick LSG film and the sheet resistance to drop from 150.37 Ω/sq to 37.58 Ω/sq. With a feed rate set to 1000 mm/min, the sheet resistance is 820 Ω sq^{-1} at 8% power, and increasing the power to 18% reduces the sheet resistance to 30Ω sq^{-1}. These results align with previous research findings that the laser power absorbed by the polyimide film directly influences the conductivity of LSG [28,29]. To balance the conductivity and durability of the device, the optimal LSG engraving parameters were determined to be a laser power range of 10% and 12% with a laser feed rate of 1000 mm/min. These parameters were used for the fabrication of the high-conductive source, drain, and gate electrodes in the OECT.

The original LSG directly machined by laser is hydrophobic with a contact angle of 71.8°, as shown in **Figure 2(a)**. The hydrophobic property of LSG limits the sensing performance when interacting with aqueous analytes. On the other hand, it affects the diffusion and adhesion of surface modifiers for selective sensing, as most modifying molecules dissolve in aqueous solutions. To address the issue, oxygen plasma treatment is conducted to convert the LSG surface to hydrophilic. After oxygen plasma, the contact angle can be significantly reduced to below 10°, as shown in **Figure 2(b)**. In the following gate modification, we also found that the measurement sensitivity significantly improved due to better diffusion of modifying solutions on LSG after oxygen plasma treatment. In addition, the oxygen plasma treatment also enhances the hydrophilic properties of the polyimide film, leading to increased adhesion between the polyimide and the channel material (PEDOT:PSS).

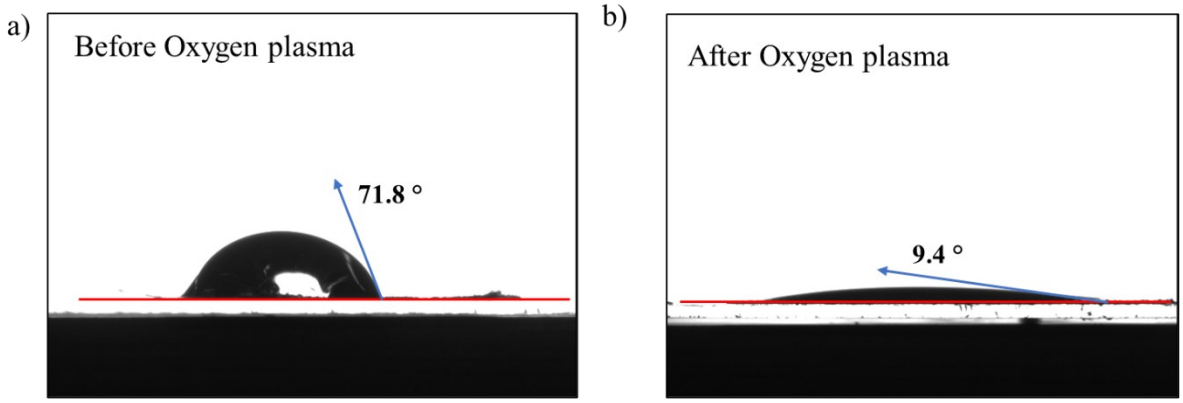

Figure 2. Contact angle measurements of LSG: a) before oxygen plasma treatment and b) after Oxygen plasma treatment.

The working principle of an OECT is based on changes in the doping state of the semiconductor channel material due to electrolyte-ion injections, thereby alternating the electrical conductivity. In this paper, the PEDOT:PSS is employed for the channel materials of the OECT. The PEDOT:PSS is a well-known semi-conductive polymer composed of p-type poly(3,4-ethylenedioxythiophene) doped with negative polystyrene sulfonate. The PEDOT: PSS can be dissolved in an aqueous solution, which is suitable for many conventional manufacturing methods[30], such as spin-coating [31], dip coating [32], and ink printing [33]. When a positive voltage is applied, it leads to the diffusion of cations (M+) from the electrolyte due to electrostatic repulsion and penetrates into the polymer matrix, which binds to holes in the channel, thus decreasing the conductivity [34]. This working mode is known as "depletion mode". At this time, PEDOT:PSS OECT enters into a neutral state, leading the transistor to shift from an "on" to an "off" state. Conversely, the opposite effect is observed when the negative gate voltage is applied, reverting the transistor return to the "on" state. This procedure can be expressed by a charge balancing equation in Equation (2):

$$\boldsymbol{PEDOT^+ :^- PSS + M^+ + e^- \Leftrightarrow PEDOT^0 + M^+ :^- PSS} \quad (2)$$

The PEDOT:PSS was prepared by adding additives to enhance its conductivity, printability, and stability (details provided in Section 4). The PEDOT:PSS was printed between the source and drain as a channel using a commercial direct ink writing printer (Zmotion®). The resulting LSG-based dual-gate OECT is shown in **Figure 1(b)**. The laser fabrication of the LSG electrodes takes approximately one minute. The most time-consuming part of the process is waiting for the PEDOT:PSS ink to fully cure. Overall, the fabrication process is straightforward, making it suitable for future modifications of the gate for customizable biosensing applications.

OECTs as amplifiers can convert low gate voltage signals into larger drain current changes. The transfer curves (I_d-V_{gs}) for a constant V_{ds} illustrate the relationship between the drain

current and the gate voltage, providing a simple means of visualizing a transistor switching from "on state" (high drain current) to "off state " (very low current) in depletion mode. Before modifying the gate surfaces for NTs sensing, the OECT was characterized in Keithley 4200-SCS with a probe station, as shown in **Figures 3(a) and (b)**. A drop of phosphate-buffered saline (PBS) (pH 7.4) was used as the electrolyte and placed between the channel and gate. **Figure 3(a)** demonstrates that the transconductance of the OECT decreases as gate voltage increases, indicating a gradual stabilization of cations diffusing from the electrolyte into the semiconductor. In terms of I_{DS}-V_D Output curves, **Figure 3(b)** shows that for different gate voltages, a higher drain voltage leads to the saturation of the drain current. Additionally, the drain current decreases with increasing gate voltage, confirming that PEDOT:PSS operates in depletion mode. Compared to other transistors, especially OTFTs that require up to tens of volts, OECTs require very low turn-off voltages. This demonstrates that LSG-based OECTs are low-power consumption devices that are suitable for portable electronic applications.

The flexibility of the LSG-based OECT was evaluated by subjecting it to drastic bending with two fingers, as shown in **Figure 2(c)**. After twenty cycles of bending and twisting in different directions, the OECT retained its morphology. The I_{ds}-V_g curves remained comparable to those observed without bending. The result indicates that the LSG-based OECT possesses high flexibility and stability, making it an ideal candidate for flexible biosensing applications.

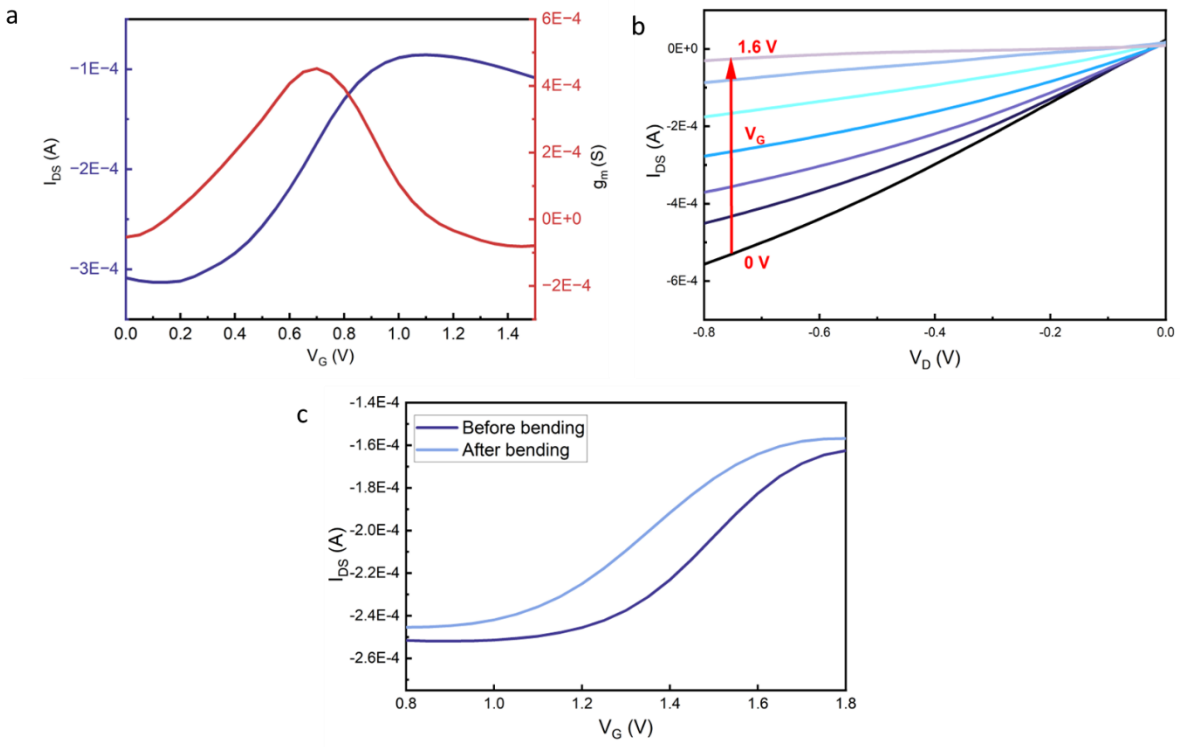

Figure 3. a) Transfer curve of LSG-based OECT (V_d= -0.3 V). b) I_{DS}-V_D output curves of LSG-based OECT (V_g= 0 to 1.6 V, step= 0.01 V). c) Transfer curve of the LSG-based OECT before and after bending (V_d= -0.4 V).

2.2 Gate Surface Modification for NT Sensing

To selectively measure specific biomolecules, the gate surface can be modified with biocompatible polymers or enzymes for customized biosensing. In this study, two significant NTs, dopamine and glutamate, are chosen as the targeted analytes detected by our LSG-based dual gate OECT. As a proof of concept, the LSG gates are modified using biopolymer for dopamine detection and L-Glutamate oxidase enzyme modification for glutamate detection.

In the animal's body, dopamine often coexists with ascorbic acid (AA) and uric acid (UA). AA and UA have close oxidation potentials to dopamine and cause peak overlap in electrochemical measurements, which are the major interfering substances. According to Wang et al. research [35], chitosan-modified graphene electrodes are highly effective in minimizing interference from AA and UA during electrochemical detection. This occurs due to the strong π-π interactions between the phenyl structure of dopamine and the two-dimensional hexagonal carbon lattice of graphene, which in turn weaken the π-π interactions between AA/UA and the graphene surface [36]. On the other hand, the photothermal process used to prepare LSG on polyimide causes the rearrangement of aromatic structures, resulting in the formation of a graphitic structure with a hexagonal carbon lattice similar to that of graphene [37]. Therefore, biopolymer chitosan (Chit) is selected to modify the LSG to further improve its selectivity. Chit is a naturally derived polysaccharide with good biocompatibility, flexibility, non-toxicity, and excellent film-forming ability. Chit polymer chains contain primary amino groups, allowing control over water solubility by adjusting the pH and ionic strength of the solution. The interaction between Chit and graphene is driven by the protonated amino groups of chitosan forming chemical bonds with the carboxyl or hydroxyl groups on the nanoparticles, thereby enhancing the water solubility and dispersion of hydrophobic nanoparticles.

The dopamine sensor functions by electro-oxidizing dopamine to o-dopamine quinone on the surface of the gate electrode. **Figure 4(a)** shows the electrooxidation process on the surface of Chit-modified LSG gate. This oxidation reaction generates electrons, which then transfer to the gate electrode, leading to an increase in effective gate voltage (V_G^{eff}). The effective gate voltage can be expressed according to the following equations [19]:

$$V_G^{eff} = V_G + 2.30(1+\gamma)\frac{KT}{2e}\log\left[C_{dopamine}\right] + Constant \quad (3)$$

Where γ is the capacitance ratio, defined as $\gamma = C_C/C_G$, C_C is the channel capacitance and C_G is the gate capacitance; k is Boltzmann's constant; T is the temperature; e is the elementary charge; and [$C_{dopamine}$,] is the molar concentration of dopamine; and V_{offset} is the offset voltage. V_G^{eff} is the equivalent voltage that needs to be applied in the absence of the Faraday effect on the gate electrode in order to produce the same source-drain current. In other words, as the concentration of dopamine increases, V_G^{eff} requires more equivalent voltage to be applied, which correspondingly decreases the source-drain current.

For comparison, cyclic voltammograms (CV) measurements were conducted to compare Chit-modified LSG gates in pure PBS solution and PBS solution with dopamine. In pure PBS, as shown by the red line in **Figure 4(b)**, no redox reactions were observed. However, upon the addition of dopamine to the PBS solution, distinct redox current peaks appeared (blue line), corresponding to oxidation and reduction reactions on the surface of the modified LSG gates. This indicates that the modified LSG electrode exhibits strong electrocatalytic activity towards dopamine, serving as redox-active molecules.

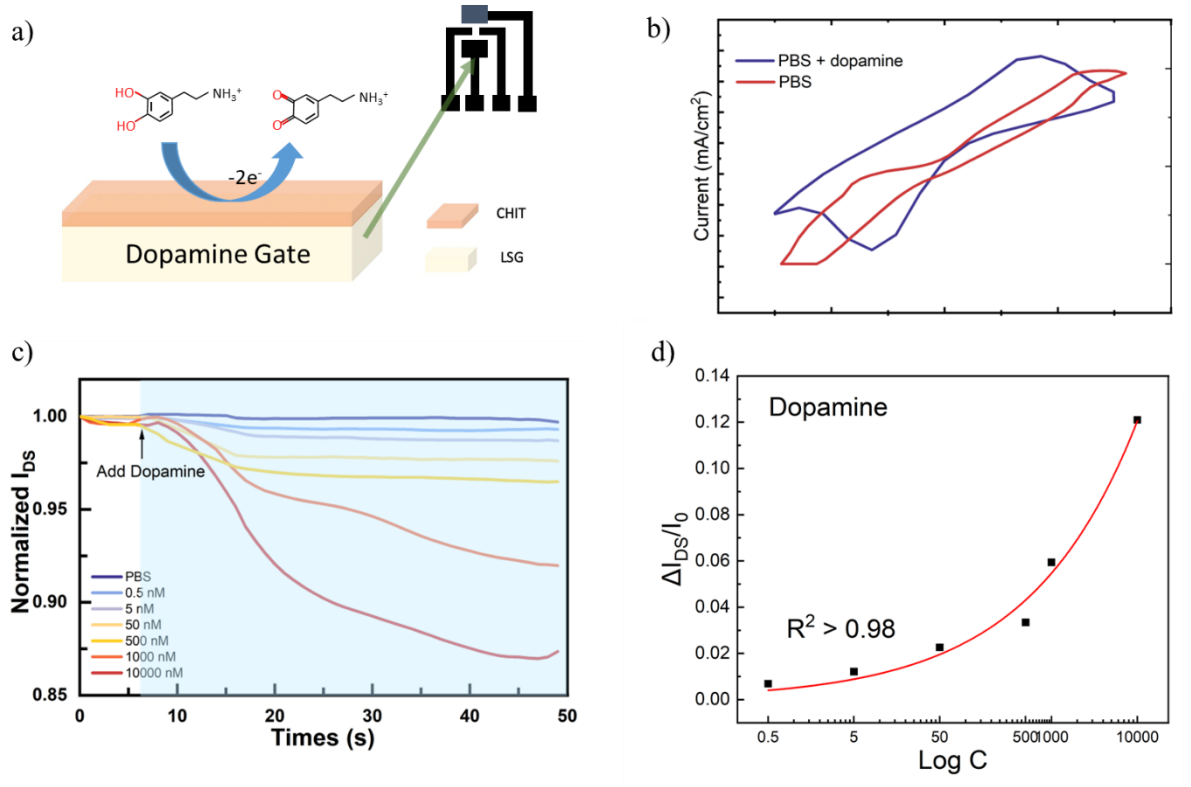

Figure 4. a) Illustration of the electrooxidation of dopamine occurs on the surface of the Chit-modified LSG gate. b) Cyclic voltammograms (CV) of Chit-modified LSG gate in the PBS solution with and without dopamine. c) Response of an OECT with the Chit-modified LSG gate electrode to additions of dopamine in PBS solution (V_d=-0.1V and V_g=0.4V). d)

Response of the normalized ΔI_{DS} in the LSG-based OECT to the logarithm of dopamine concentration.

In this paper, we also demonstrated the quantitative detection of dopamine using Chit-modified LSG-based OECT. **Figure 4(c)** shows the real-time normalized drain current response of the OECT with Chit-modified gate to the addition of dopamine. The normalized current (NC) was calculated with Equation (4) to facilitate the comparison between different concentration responses, where $I_D(Con0)$ is the current before the addition of the NTs, and $I_D(Conc)$ is the current after adding the NTs to the gate:

$$NC = \left|\frac{I_D(Con0)}{I_D(Conc)}\right| \tag{4}$$

In the experiment, the dopamine concentrations were increased from 0.5 nM, 5 nM, 50 nM, 500 nM, and 1000 nM, to 10,000 nM. As we applied a positive V_g (0.4V), the gate potential is higher than the electrochemical potential of the source, promoting dopamine oxidation at the gate. When dopamine was detected, the drain current of OECT dropped quickly within 5s. This drop in drain current was strongly correlated to the concentration of the detected dopamine solution. Experimental results show that the OECT's minimum detection limit for dopamine is approximately 5 nM. Additionally, the normalized current variation increases when the concentration exceeds 1,000 nM. This can be explained by the presence of an oxidizable dopamine in the solution, which acts as an 'extra gate,' further inhibiting the OECT channel. As dopamine concentration rises, it becomes increasingly difficult for current to flow through the channel, causing the transfer curves to shift downward with increasing dopamine levels. Quantitatively, ΔI_d was fitted exponentially with a coefficient $R^2 > 0.98$ over the range of 0.5 nM to 10,000 nM in **Figure 4(d).** However, there is a near linear relationship over the concentration range of 50 nM to 10,000 nM demonstrates the ability to detect a broad range of dopamine concentrations.

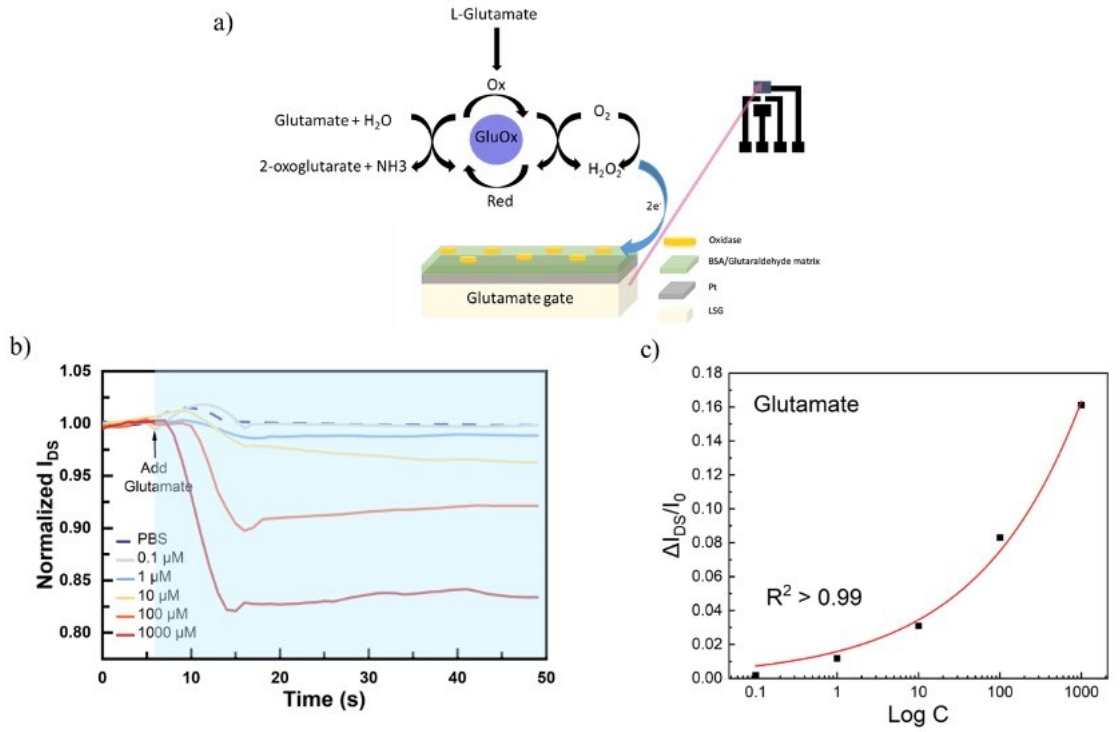

Figure 5. a) Illustration of the electrooxidation of enzymatic sensing occurs on the surface of the modified LSG gate. b) Response of an OECT with the enzyme-modified LSG gate electrode to additions of glutamate in PBS solution (V_d=-0.1V and V_g=0.4V). b) Response of the normalized ΔI_{DS} in the LSG-based OECT to the logarithm of glutamate concentration.

In addition to modifying the LSG gate with biopolymers, we also investigate enzymatic modification of the LSG gate for glutamate detection. **Figure 5(a)** shows the electrooxidation process of the glutamate. Glutamate is oxidized to 2-oxoglutarate with GluOx acting as an oxidoreductase, transferring the lost electrons to oxygen. This results in the reduction of oxygen to H_2O_2, which is subsequently electrochemically sensed by OECT. While the charge transfer of H_2O_2 is slow on most conductive substrates, platinum (Pt) exhibits excellent electrocatalytic activity toward H_2O_2 [38]. Therefore, Pt particles were sputtering deposited on the LSG gate first, then modified by crosslinking the enzyme solution on the gate, as shown in **Figure 5(a).** The porous structure and large surface area of LSG can increase the number of effective catalytic sites and expand the area of oxidation reaction after Pt deposition. Additionally, the inherent high conductivity of LSG provides a good pathway for electron transfer.

Figure 5(b) shows the real-time normalized drain current response of the OECT with enzyme-modified gate to the addition of glutamate. As shown in **Figure 5(b),** glutamate was quantitatively detected within the range of 0.1 μM to 1000 μM (0.1 μM, 1 μM, 10 μM, 100 μM, and 1000 μM). Experimental results present that the OECT's minimum detection limit for

glutamate is approximately 1 μM. The detection response time was slightly longer than the biopolymer-modified gate for DA in **Figure 4(c)**, possibly due to the slow binding and enzymatic reaction of glutamate. Quantitatively, ΔI_d was fitted exponentially with a coefficient $R^2 > 0.99$ over the range of 1 μM to 1000 μM in **Figure 5(c)**. It is infinitely close to 0 at 0.1 μM, and exhibits a linear relationship in the range of concentrations from 1 μM to 1000 μM, demonstrating that OECT is suitable for detecting low concentrations of glutamate with a broad range.

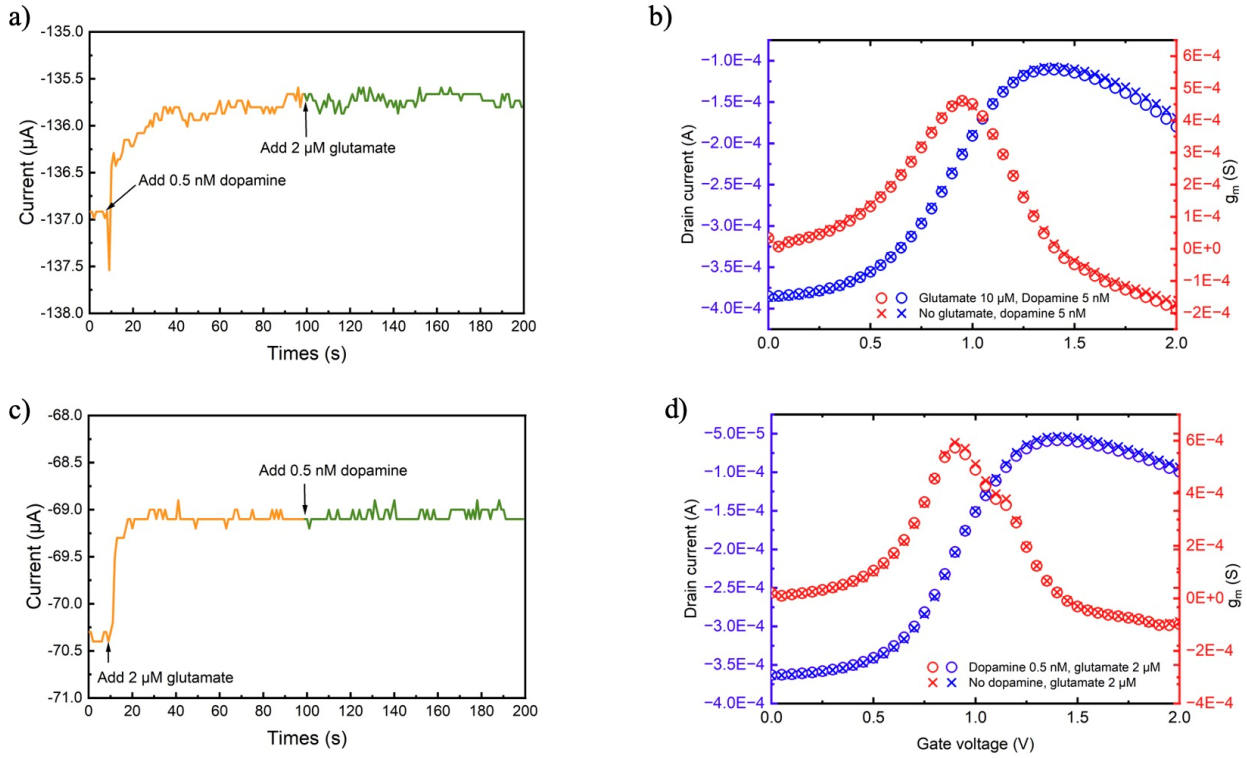

Figure 6. a) Chronoamperometry experiment for dopamine sensing (add 5 nM dopamine first and add 10μm glutamate at 100s, V_d=-0.1V and V_g=0.4V). b) I_d-V_{gs} of 5nM dopamine, and both 5 nM dopamine and 10 μM glutamate (V_d= -0.6 V). c) Chronoamperometry experiment for glutamate sensing (add 2 μM glutamate first, and add 0,5 nM dopamine at 100s, V_d=-0.1V and V_g=0.4V). d) I_d-V_{gs} of 2 μm dopamine, and both 0.5 nM dopamine and 2 μM glutamate (V_d= -0.6 V).

Due to the high selectivity achieved through gate modification, the LSG-based dual-gate OECT is well-suited for more complicated analyses, enabling independent and isolated detection by switching the gate, thereby sensing the two NTs without interference. During the detection, the constant V_d=-0.1V and V_g=0.4V are applied to the OECT, and only switching the connection of gate electrode to measure the two NTs. Thanks to the high selectivity of the chitosan/enzyme-modified gate, it can independently detect dopamine and glutamate without

interference, even when the analyte solution including both compounds are present on both gates at the same time. In order to validate this, **Figure 6** shows a chronoamperometry experiment designed to examine potential interference during the detection of the two NTs. In **Figure 6(a),** 5 nM of dopamine was initially added to Chit-modified OECT, causing a quick and obvious responsive current. Subsequently, 10 μM of glutamate was added at 100 seconds, while almost no change was observed in the dopamine sensing current. This indicates that the glutamate did not interact with the dopamine-sensitive gate. To further validate this, the I_d-V_{gs} transfer curves were compared by adding 5 nM of dopamine followed by the addition of 10 μM of glutamate, with the same drain voltage (-0.3 V), as shown in **Figure 6(b)**. The comparison of transfer curves for dopamine alone and two NTs (dopamine and glutamate) shows minimal change in the transfer curves. This also demonstrates that the presence of multiple analytes in the electrolyte does not affect the detection of dopamine by the Chit-modified gate.

A similar validation experiment was also conducted for enzyme-modified OECT. 2 μM of glutamate was first added, followed by a subsequent addition of 0.5 nM of dopamine at 100 seconds. **Figure 6(c)** presents no influence on the glutamate sensing current after adding dopamine. In other words, the dopamine would not affect the enzymatic reaction and electrooxidation on the modified gate surface. For the transfer curves, the comparison demonstrates that the addition of dopamine would not affect the detection of glutamate. These results indicate that there is no crosstalk between the gates, confirming that the LSG-based dual-gate OECT is suitable for the simultaneous analysis of multiple NTs.

3. Conclusions

In this paper, we successfully designed and fabricated a dual-gate organic electrochemical transistor (OECT) using laser-scribed graphene (LSG) for the simultaneous detection of dopamine and glutamate. The LSG electrodes can be easily fabricated using a benchtop laser cutter on the polyimide thin film. By optimizing the scribing parameters, the LSG can achieve an impedance comparable to that of traditional gold electrodes. Thanks to the planar device architecture, a flexible dual-gate OECT can be designed to detect multiple chemicals by modifying the gate with minimal interference. As proof of concept, we successfully modified one gate with biopolymer chitosan for dopamine detection and the other gate with L-Glutamate oxidase enzyme for glutamate detection. The developed dual-gate OECT shows outstanding sensing performance with detection limits of 5 nM for dopamine and 0.1 μM for glutamate. This dual-gate OECT demonstrates significant potential for use in complex biosensing applications, particularly in diagnosing and monitoring neurological disorders. In terms of cost and manufacturing, OECT with LSG has significant advantages over conventional devices that

use precious metal materials and mask-based fabrication. The scalability and customizability of LSG-based OECTs also open the door to broader applications in multi-analyte sensing beyond neurotransmitter detection.

4. Experiment Section

***PEDOT:PSS Preparation*:** Commercial pristine 1.3 wt.% PEDOT:PSS (Pedotinks®) was used with 3 wt.% of dimethyl sulfoxide (DMSO) (Sigma-Aldrich). 1 wt.% (3-glycidyloxypropyl) trimethoxy silane (GOPS) (Sigma-Aldrich) was added into the PEDOT:PSS ink to make it insoluble in aqueous solutions after drying. To improve the printability, 0.1 wt.% dodecyl benzene sulfonic acid (DBSA) (Sigma-Aldrich) was also added. The mixed PEDOT:PSS ink was evenly stirred for 2 hours before printing.

Chitosan and Dopamine Solutions Preparation: 0.5 g of chitosan (Sigma-Aldrich) was first dissolved in 100 mL of 50 mM acetic acid solution (pH=5-6) (Sigma-Aldrich) and then sonicated for one hour to be fully dissolved in the aqueous solution. In order to examine the response of different concentrations of dopamine, we added corresponding weights of dopamine (Sigma-Aldrich) to 200 mL of PBS (Sigma-Aldrich) solution to mix into a dopamine electrolyte, and all of the above solutions were stored in a refrigerator at 4 °C for 24 hours.

L-Glutamate Oxidase Enzyme Preparation: we dissolved 0.1UmL^-1 of glutamate oxidase in 10 ml of Potassium. Then 20 ul of L-Glutamate oxidase enzyme solution was added to 100 ul of PBS. 4ul of Glutaraldehyde solution (50% wt) was taken and first diluted into 76ul of deionized water, 2.5 mg of BSA was added to 10ul of Glutaraldehyde solution (2.5% wt), and finally mixed and added to 120ul of fixation solution. In order to examine the response of different concentrations of glutamate, we added corresponding concentrations of L-glutamate monosodium salt (98% purity from Sigma-Aldrich) to PBS solution as an electrolyte.

Dual-gate OECT Fabrication: A commercial Kapton® Polyimide (PI) thin film with a thickness of 0.0010” was attached on a glass slide (Vabiooth, thickness 1mm - 1.2mm) using water-washable TEQStone® adhesive glue to ensure the flatness of the PI film and prevent thermal deformation during the laser engraving. To fabricate the LSG on the PI, a benchtop 5W UV laser cutter was employed to engrave CAD-designed OECT patterns. To improve the wettability of LSG and PI, The Plasma Cleaner PDC-32g was used to perform oxygen plasma on the LSG for 5 minutes. The PEDOT:PSS channel was printed between the source and drain electrodes. After printing, we cured the PEDOT:PSS on a hotplate at 120°C for 1 hour for fully crosslink. A paper mask was made to cover the OECT and only expose the bottom gate. The Pt particles were then deposited via sputtering. The chitosan was drop-casted on the top gate of

OECT. L-Glutamate oxidase enzymes were drop-casted on the bottom gate of OECT, dried at room temperature for 24hrs and then washed with PBS to remove impurities. Finally, PI tapes were used to cover the OECT and only expose the channel and gate areas for sensing.

Characterizations: The resistivity of the LSG fabricated with different powers and feed rates was measured using a Keithley 2400 SourceMeter with a four-point probe stand (302 resistivity probe stand). Output and transfer characteristics of OECT were measured using a Keithley 4200A-SCS parametric analyzer with a probe station. Cyclic voltammetry of dopamine was tested using a Keithley 2450 SourceMeter with Pt foil as the counter electrode, Ag/AgCl electrode as the reference electrode, and a CV scan rate of 50mV/s. Keithley 2450 SourceMeter and a Keithley 2400 SourceMeter were used for the chronoamperometry. The contact angle before and after oxygen plasma with drops of chit solution on LSG was tested using a Ramé-hart Model 250.

Acknowledgments

The authors gratefully acknowledge the financial support from the National Science Foundation (NSF) through Award No. CBET-2336525 and College of Engineering Seed Grant at the University of Missouri.

Conflict of Interest

The authors declare no conflict of interest.

Keywords

OECT, LSG, PEDOT:PSS, Neurotransmitters, Dopamine, Glutamate, Neural Chemical Sensors

Reference

[1] E. T. Kavalali, *Nat Rev Neurosci* **2015**, *16*, 5.
[2] Y. Zhou, N. C. Danbolt, *J Neural Transm* **2014**, *121*, 799.
[3] R. M. Guerriero, C. C. Giza, A. Rotenberg, *Current neurology and neuroscience reports* **2015**, *15*, 1.
[4] J. E. Ahlskog, *Neurology* **2007**, *69*, 1701.
[5] J. V. Andersen, K. H. Markussen, E. Jakobsen, A. Schousboe, H. S. Waagepetersen, P. A. Rosenberg, B. I. Aldana, *Neuropharmacology* **2021**, *196*, 108719.
[6] S. Ikemoto, *Brain research reviews* **2007**, *56*, 27.
[7] D. F. Fiorino, A. Coury, H. C. Fibiger, A. G. Phillips, *Behavioural brain research* **1993**, *55*, 131.
[8] E. Gemperline, B. Chen, L. Li, *Bioanalysis* **2014**, *6*, 525.
[9] H.-M. Zhang, N.-Q. Li, Z. Zhu, *Microchemical Journal* **2000**, *64*, 277.

[10] H. Zhao, Y. Zhang, Z. Yuan, *Analytica Chimica Acta* **2001**, *441*, 117.
[11] P. T. Kissinger, C. Refshauge, R. Dreiling, R. N. Adams, *Analytical Letters* **1973**, *6*, 465.
[12] K. Xie, N. Wang, X. Lin, Z. Wang, X. Zhao, P. Fang, H. Yue, J. Kim, J. Luo, S. Cui, F. Yan, P. Shi, *Organic electrochemical transistor arrays for real-time mapping of evoked neurotransmitter release in vivo*, eLife Sciences Publications Limited, **2020**.
[13] C. W. Atcherley, K. M. Wood, K. L. Parent, P. Hashemi, M. L. Heien, *Chemical Communications* **2015**, *51*, 2235.
[14] C. Zhao, K. M. Cheung, I.-W. Huang, H. Yang, N. Nakatsuka, W. Liu, Y. Cao, T. Man, P. S. Weiss, H. G. Monbouquette, A. M. Andrews, *Sci. Adv.* **2021**, *7*, eabj7422.
[15] J. Rivnay, P. Leleux, M. Ferro, M. Sessolo, A. Williamson, D. A. Koutsouras, D. Khodagholy, M. Ramuz, X. Strakosas, R. M. Owens, C. Benar, J.-M. Badier, C. Bernard, G. G. Malliaras, *Sci. Adv.* **2015**, *1*, e1400251.
[16] W. Lee, D. Kim, J. Rivnay, N. Matsuhisa, T. Lonjaret, T. Yokota, H. Yawo, M. Sekino, G. G. Malliaras, T. Someya, *Advanced Materials* **2016**, *28*, 9722.
[17] J. Rivnay, H. Wang, L. Fenno, K. Deisseroth, G. G. Malliaras, *Science Advances* **2017**, *3*, e1601649.
[18] W. Lee, D. Kim, J. Rivnay, N. Matsuhisa, T. Lonjaret, T. Yokota, H. Yawo, M. Sekino, G. G. Malliaras, T. Someya, *Advanced Materials* **2016**, *28*, 9722.
[19] D. A. Bernards, D. J. Macaya, M. Nikolou, J. A. DeFranco, S. Takamatsu, G. G. Malliaras, *J. Mater. Chem.* **2008**, *18*, 116.
[20] P. Lin, F. Yan, *Advanced Materials* **2012**, *24*, 34.
[21] Z. Yi, G. Natale, P. Kumar, E. Di Mauro, M.-C. Heuzey, F. Soavi, I. I. Perepichka, S. K. Varshney, C. Santato, F. Cicoira, *Journal of Materials Chemistry C* **2015**, *3*, 6549.
[22] A. Ait Yazza, P. Blondeau, F. J. Andrade, *ACS Appl. Electron. Mater.* **2021**, *3*, 1886.
[23] S. Y. Park, S. Y. Son, I. Lee, H. Nam, B. Ryu, S. Park, C. Yun, *ACS Appl. Mater. Interfaces* **2024**, *16*, 46664.
[24] X. Xi, D. Wu, W. Ji, S. Zhang, W. Tang, Y. Su, X. Guo, R. Liu, *Adv Funct Materials* **2020**, *30*, 1905361.
[25] S. Y. Yeung, X. Gu, C. M. Tsang, S. W. Tsao, I. -ming Hsing, *Sensors and Actuators A: Physical* **2019**, *287*, 185.
[26] L. Wang, X. Yue, Q. Sun, L. Zhang, G. Ren, G. Lu, H.-D. Yu, W. Huang, *Nano Res.* **2022**, *15*, 2433.
[27] V. Strong, S. Dubin, M. F. El-Kady, A. Lech, Y. Wang, B. H. Weiller, R. B. Kaner, *ACS Nano* **2012**, *6*, 1395.
[28] S. Zhang, Y. Yao, Y. Wang, In *International Manufacturing Science and Engineering Conference*, American Society of Mechanical Engineers, **2023**, p. V001T03A005.
[29] M. Tavakkoli Gilavan, M. S. Rahman, A. Minhas-Khan, S. Nambi, G. Grau, *ACS Appl. Electron. Mater.* **2021**, *3*, 3867.
[30] K. Sun, S. Zhang, P. Li, Y. Xia, X. Zhang, D. Du, F. H. Isikgor, J. Ouyang, *J Mater Sci: Mater Electron* **2015**, *26*, 4438.
[31] A. M. Nardes, M. Kemerink, R. A. J. Janssen, *Phys. Rev. B* **2007**, *76*, 085208.
[32] Y. Ding, J. Yang, C. R. Tolle, Z. Zhu, *ACS Appl. Mater. Interfaces* **2018**, *10*, 16077.
[33] O. O. Olowo, R. Zhang, A. Sherehiy, B. Goulet, A. Curry, D. Wei, Z. Yang, M. Alqatamin, D. O. Popa, In *International Manufacturing Science and Engineering Conference*, American Society of Mechanical Engineers, **2022**, p. V001T07A004.
[34] S. T. Keene, T. P. A. Van Der Pol, D. Zakhidov, C. H. L. Weijtens, R. A. J. Janssen, A. Salleo, Y. Van De Burgt, *Advanced Materials* **2020**, *32*, 2000270.
[35] Y. Wang, Y. Li, L. Tang, J. Lu, J. Li, *Electrochemistry Communications* **2009**, *11*, 889.
[36] H. Bi, Y. Li, S. Liu, P. Guo, Z. Wei, C. Lv, J. Zhang, X. S. Zhao, *Sensors and Actuators B: Chemical* **2012**, *171–172*, 1132.

[37] J. Zhu, X. Huang, W. Song, *ACS Nano* **2021**, *15*, 18708.
[38] S. B. Hall, E. A. Khudaish, A. L. Hart, *Electrochimica Acta* **1998**, *43*, 579.